

# Kosterlitz-Thouless transition and vortex-antivortex lattice melting in two-dimensional Fermi gases with $p$ - or $d$ -wave pairing

Gaoqing Cao<sup>1</sup>, Liyan He<sup>2</sup> and Xu-Guang Huang<sup>1,3</sup>

<sup>1</sup> Department of Physics and Center for Particle Physics and Field Theory, Fudan University, Shanghai 200433, China

<sup>2</sup> State Key Laboratory of Low-Dimensional Quantum Physics and Department of Physics, Tsinghua University, Beijing 100084, China

<sup>3</sup> Key Laboratory of Nuclear Physics and Ion-beam Application (MOE), Fudan University, Shanghai, China 200433.

(Dated: December 14, 2024)

We present a theoretical study of the finite-temperature Kosterlitz-Thouless (KT) and vortex-antivortex lattice (VAL) melting transitions in two-dimensional Fermi gases with  $p$ - or  $d$ -wave pairing. For both pairings, when the interaction is tuned from weak to strong attractions, we observe a quantum phase transition from the Bardeen-Cooper-Schrieffer (BCS) superfluidity to the Bose-Einstein condensation (BEC) of dfermions. The KT and VAL transition temperatures increase during this BCS-BEC transition and approach constant values in the deep BEC region. The BCS-BEC transition is characterized by the non-analyticities of the chemical potential, the superfluid order parameter, and the sound velocities as functions of the interaction strength at both zero and finite temperatures; however, the temperature effect tends to weaken the non-analyticities comparing to the zero temperature case. The effect of mismatched Fermi surfaces on the  $d$ -wave pairing is also studied.

## I. INTRODUCTION

It was proposed by Eagles [1] and Leggett [2] several decades ago that, in a many-fermion system with attractive interaction, one can realize an evolution from the Bardeen-Cooper-Schrieffer (BCS) superfluidity to Bose-Einstein condensation (BEC) of dfermion molecules by gradually increasing the strength of the interaction. For  $s$ -wave interaction, such a BCS- BEC evolution is a smooth crossover [3–11] which has been experimentally studied by using the dilute ultracold fermionic atoms [15–17], where the interaction strength is tuned by means of the Feshbach resonance. Such a dilute ultracold atomic system is characterized by a dimensionless parameter  $1/(k_F a_s)$ , where  $a_s$  is the  $s$ -wave scattering length of the short-range interaction and  $k_F$  is the Fermi momentum in the absence of interaction. The BCS-BEC crossover occurs when  $1/(k_F a_s)$  goes from  $-\infty$  to  $\infty$ . In addition, the Anderson-Bogoliubov collective mode of fermionic superfluidity at weak attraction evolves smoothly to the Bogoliubov excitation of weakly repulsive Bose condensate at strong attraction [5, 11–14].

On the other hand, for nonzero orbital-angular-momentum pairing, such as  $p$ - or  $d$ -wave pairing, the BCS-BEC evolution is not smooth but associated with some quantum phase transition[18–25]. Such a quantum phase transition cannot be characterized by a change of symmetry or the associated order parameter. Instead, different quantum phases can be distinguished topologically [18]. Two-dimensional (2D) systems are of particular interest since the topological  $p$ -wave pairing state exhibits nonabelian statistics [18] and hence is useful for topological computation. In cold-atom experiments, a quasi-2D Fermi gas can be realized by arranging a one-dimensional optical lattice along the axial direction and a weak harmonic trapping potential in the radial plane, such that fermions are strongly confined along the axial direction and form a series of pancake-shaped quasi-2D clouds [26–30].

For 2D fermionic systems with generic  $p$ -or  $d$ -wave pairing at zero temperature, the thermodynamic quantities and the velocity of the low-energy collective mode can be non-analytic

functions of the two-body binding energy at the BCS-BEC quantum phase transition point where the chemical potential vanishes [19, 20, 25]. Interestingly, these non-analyticities are determined solely by the infrared behavior of the interaction potential, i.e., independent of the details of the interaction potential as well as the symmetry associated with the order parameter [25]. However, the temperature in a realistic ultracold atomic gas is always nonzero. Therefore, it is important to study how these non-analyticities are modified when the temperature is nonzero. In addition, it is well known that the thermal superfluid transition in 2D becomes of the Kosterlitz-Thouless (KT) type and vortex-antivortex lattice (VAL) may also exist at low temperature [33–35]. It is thus necessary to study the KT and VAL transitions in 2D fermionic systems with  $p$ -or  $d$ -wave pairing. The KT and VAL transitions has been comprehensively studied for 2D Fermi gases with  $s$ -wave pairing [36–43] and with spin-orbit coupling [44–48].

In this work, we present a systematical study of the KT and VAL melting transitions in 2D Fermi gases with  $p$ - or  $d$ -wave pairing. We find that the non-analyticities are weakened by finite-temperature effect. In particular, we calculate the sound velocity  $v$  as a function of temperature and interaction strength (the two-body binding energy). For the  $p$ -wave pairing,  $v$  is a non-monotonous function of the two-body binding energy, while for the  $d$ -wave pairing,  $v$  decreases monotonously with the binding energy. The effect of mismatched Fermi surfaces is also studied for the  $d$ -wave pairing. In the BEC regime, we find that the KT and VAL transition temperature both decrease linearly for large chemical potential imbalance, and a superfluid-normal phase transition occurs when the imbalance reaches a critical value.

The paper is arranged as follows. We present the study of  $p$ -wave pairing system and  $d$ -wave pairing system in Sec.II and Sec.III, respectively. The theoretical formalism is given in Sec.II A and Sec.III A. The numerical results are given in Sec.II B for  $p$ -wave pairing and in Sec.III B for  $d$ -wave pairing. Finally, we summarize in Sec.IV. We use the natural units  $\hbar = k_B = 1$  throughout.

## II. *p*-WAVE PAIRING IN SPINLESS FERMI GASES

### A. Formalism in Gaussian approximation

Since the fermion wave function should be anti-symmetric, the simplest setup to study *p*-wave pairing is a “spinless” Fermi gas, or single-component Fermi gas. The Hamiltonian can be written as [18, 19]

$$\mathcal{H} = \sum_{\mathbf{k}} \psi_{\mathbf{k}}^\dagger \xi_{\mathbf{k}} \psi_{\mathbf{k}} + \sum_{\mathbf{k}, \mathbf{k}', \mathbf{q}} V_{\mathbf{k}\mathbf{k}'}^p b_{\mathbf{k}\mathbf{q}}^\dagger b_{\mathbf{k}'\mathbf{q}}, \quad (1)$$

where  $\psi_{\mathbf{k}}$  represents the fermion annihilation operator,  $b_{\mathbf{k}\mathbf{q}} = \psi_{-\mathbf{k}+\mathbf{q}/2} \psi_{\mathbf{k}+\mathbf{q}/2}$ , and  $\xi_{\mathbf{k}} = \epsilon_{\mathbf{k}} - \mu$  with the kinetic energy  $\epsilon_{\mathbf{k}} = \mathbf{k}^2/(2m)$ . For the sake of simplicity, we consider a separable *p*-wave interaction potential  $V_{\mathbf{k}\mathbf{k}'}^p$  [25],

$$V_{\mathbf{k}\mathbf{k}'}^p = -\lambda \Gamma^p(\mathbf{k}) \Gamma^{p*}(\mathbf{k}'), \quad (2)$$

where  $\lambda$  is the interaction strength. The gamma functions takes the Nozieres-Schmitt-Rink (NSR) form [3, 19],

$$\Gamma_s^p(\mathbf{k}) = \frac{(k_x + ik_y)/k_1}{(1 + k/k_0)^{3/2}}, \quad \Gamma_a^p(\mathbf{k}) = \frac{k_x/k_1}{(1 + k/k_0)^{3/2}}, \quad (3)$$

with  $k = |\mathbf{k}|$ . Here *s* and *a* represent the symmetric (isotropic)  $p_x + ip_y$  and asymmetric (anisotropic)  $p_x$  pairings, respectively. The parameters  $k_0$  and  $k_1$  set the momentum scale in the short and long wavelength limits, respectively [19]. The form of the denominator is chosen to mimic the amplitude damping for *p*-wave partial potential at large momentum [19].

The partition function at finite temperature can be given by the imaginary-time path integral formalism,

$$\mathcal{Z} = \int [d\psi^\dagger] [d\psi] \exp \left\{ - \int_0^\beta d\tau \left( \sum_{\mathbf{k}} \psi_{\mathbf{k}}^\dagger \partial_\tau \psi_{\mathbf{k}} + \mathcal{H} \right) \right\}, \quad (4)$$

where  $\tau = it$  is the imaginary time and  $\beta = 1/T$  with  $T$  being the temperature. Introducing an auxiliary bosonic field  $\phi_{\mathbf{q}}(\tau) = 2\lambda \sum_{\mathbf{k}} \Gamma^p(\mathbf{k}) b_{\mathbf{k}\mathbf{q}}$  and applying the Hubbard-Stratonovich transformation, we can rewrite the partition function as

$$\mathcal{Z} = \int [d\phi^*] [d\phi] [d\Psi^\dagger] [d\Psi] \exp \left\{ - \int_0^\beta d\tau \left[ \sum_{\mathbf{q}} \frac{|\phi_{\mathbf{q}}(\tau)|^2}{4\lambda} + \frac{1}{2} \sum_{\mathbf{k}, \mathbf{k}'} (\xi_{\mathbf{k}} \delta_{\mathbf{k}, \mathbf{k}'} - \Psi_{\mathbf{k}}^\dagger G_{\mathbf{k}, \mathbf{k}'}^{-1} \Psi_{\mathbf{k}'}) \right] \right\}, \quad (5)$$

where we use the Nambu-Gor’kov representation  $\Psi_{\mathbf{k}}^\dagger = (\psi_{\mathbf{k}}^\dagger, \psi_{-\mathbf{k}})$ . The inverse fermion Green’s function is given by

$$G_{\mathbf{k}, \mathbf{k}'}^{-1}(\tau) = \begin{pmatrix} (-\partial_\tau - \xi_{\mathbf{k}}) \delta_{\mathbf{k}, \mathbf{k}'} & \phi_{\mathbf{k}-\mathbf{k}'}(\tau) \Gamma^p\left(\frac{\mathbf{k}+\mathbf{k}'}{2}\right) \\ \phi_{-\mathbf{k}+\mathbf{k}'}^*(\tau) \Gamma^{p*}\left(\frac{\mathbf{k}+\mathbf{k}'}{2}\right) & (-\partial_\tau + \xi_{\mathbf{k}}) \delta_{\mathbf{k}, \mathbf{k}'} \end{pmatrix}. \quad (6)$$

Integrating out the fermion degrees of freedom, we obtain

$$\mathcal{Z} = \int [d\phi^*] [d\phi] e^{-\mathcal{S}_{\text{eff}}^p[\phi^*, \phi]}, \quad (7)$$

with the effective action

$$\mathcal{S}_{\text{eff}}^p = \int_0^\beta d\tau \left[ \sum_{\mathbf{q}} \frac{|\phi_{\mathbf{q}}(\tau)|^2}{4\lambda} + \frac{1}{2} \sum_{\mathbf{k}, \mathbf{k}'} (\xi_{\mathbf{k}} \delta_{\mathbf{k}, \mathbf{k}'} - \text{Tr} \ln G_{\mathbf{k}, \mathbf{k}'}^{-1}) \right], \quad (8)$$

where the trace is taken over imaginary time, momentum and Nambu-Gor’kov spaces.

To proceed, we decompose the auxiliary field  $\phi_{\mathbf{q}}(\tau)$  into its mean-field and fluctuation parts,

$$\phi_{\mathbf{q}}(\tau) = \Delta_{\mathbf{q}, 0} + \hat{\phi}_{\mathbf{q}}(\tau). \quad (9)$$

The effective action can be evaluated in powers of the fluctuation  $\hat{\phi}_{\mathbf{q}}(\tau)$ , i.e.,  $\mathcal{S}_{\text{eff}}^p = \mathcal{S}_0^p + \mathcal{S}_2^p + \dots$ . Here we omit the linear term in the fluctuation since it vanishes due to the gap equation. The leading-order term  $\mathcal{S}_0^p$  represents the mean-field contribution. The next-to-leading-order term  $\mathcal{S}_2^p$ , which is quadratic in the fluctuation, represents the Gaussian fluctuations and hence the collective mode dynamics.

#### 1. Mean-field approximation

The mean-field contribution  $\mathcal{S}_0^p$  can be evaluated as

$$\begin{aligned} \mathcal{S}_0^p &= \beta S \left[ \frac{\Delta^2}{4\lambda} + \frac{1}{2} \int \frac{d^2 \mathbf{k}}{(2\pi)^2} \xi_{\mathbf{k}} - \frac{T}{2} \sum_n \int \frac{d^2 \mathbf{k}}{(2\pi)^2} \ln \det \mathcal{G}_{\mathbf{k}}^{-1}(i\omega_n) \right] \\ &= \beta S \left\{ \frac{\Delta^2}{4\lambda} - \frac{1}{2} \int \frac{d^2 \mathbf{k}}{(2\pi)^2} [E_{\mathbf{k}} - \xi_{\mathbf{k}} + 2T \ln(1 + e^{-E_{\mathbf{k}}/T})] \right\}, \end{aligned} \quad (10)$$

where  $S$  is the area of the system and  $\omega_n = (2n + 1)\pi T$  ( $n \in \mathbb{Z}$ ) is the fermion Matsubara frequency. The inverse fermion Green’s function in mean-field approximation is given by

$$\mathcal{G}_{\mathbf{k}}^{-1}(i\omega_n) = \begin{pmatrix} i\omega_n - \xi_{\mathbf{k}} & \Delta_{\mathbf{k}}^p \\ \Delta_{\mathbf{k}}^{p*} & i\omega_n + \xi_{\mathbf{k}} \end{pmatrix}, \quad (11)$$

which gives the fermionic quasiparticle spectrum  $E_{\mathbf{k}} = (\xi_{\mathbf{k}}^2 + |\Delta_{\mathbf{k}}^p|^2)^{1/2}$  with  $\Delta_{\mathbf{k}}^p = \Delta \Gamma^p(\mathbf{k})$ . The mean field  $\Delta$ , normally referred to as the superfluid order parameter, is determined by the extreme condition  $\partial \mathcal{S}_0^p / \partial \Delta = 0$ , which gives rise to the gap equation

$$\frac{1}{\lambda} = \int \frac{d^2 \mathbf{k}}{(2\pi)^2} \frac{|\Gamma^p(\mathbf{k})|^2}{E_{\mathbf{k}}} \tanh\left(\frac{E_{\mathbf{k}}}{2T}\right). \quad (12)$$

The mean-field contribution to the number density is obtained through the thermodynamic relation  $n_0 = -(\partial \mathcal{S}_0^p / \partial \mu) / (\beta S)$ . We have

$$n_0 \equiv \int \frac{d^2 \mathbf{k}}{(2\pi)^2} n_0(\mathbf{k}) = \frac{1}{2} \int \frac{d^2 \mathbf{k}}{(2\pi)^2} \left[ 1 - \frac{\xi_{\mathbf{k}}}{E_{\mathbf{k}}} \tanh\left(\frac{E_{\mathbf{k}}}{2T}\right) \right]. \quad (13)$$

The interaction strength  $\lambda$  can be physically characterized by the two-body binding energy  $E_b$  in vacuum. It is given by [19]

$$\frac{1}{\lambda} = \int \frac{d^2 \mathbf{k}}{(2\pi)^2} \frac{2|\Gamma^p(\mathbf{k})|^2}{2\epsilon_{\mathbf{k}} - E_b}. \quad (14)$$

Note that unlike the *s*-wave case, here the binding energy  $E_b$  can be both negative or positive. The weak and strong attraction limits correspond to  $E_b \rightarrow +\infty$  and  $E_b \rightarrow -\infty$ , respectively.

## 2. Gaussian fluctuation and Goldstone mode

The Gaussian fluctuation contribution to the effective action is quadratic in  $\phi_{\mathbf{q}}(\tau)$  and thus represents the collective mode dynamics. It can be evaluated as

$$\mathcal{S}_2^p = \sum_{\mathbf{q}, n} \left\{ \frac{|\hat{\phi}_{\mathbf{q}}(iv_n)|^2}{4\lambda} + \frac{T}{4S} \sum_{\mathbf{k}, m} \text{Tr} \left[ \mathcal{G}_{\mathbf{k}-\mathbf{q}/2}(i\omega_m) \right. \right. \\ \left. \times \Phi_{-\mathbf{q}}(-iv_n) \mathcal{G}_{\mathbf{k}+\mathbf{q}/2}(i\omega_m + iv_n) \Phi_{\mathbf{q}}(iv_n) \right] \right\}, \quad (15)$$

where  $\nu_n = 2\pi nT$  ( $n \in \mathbb{Z}$ ) is the boson Matsubara frequency, and the mean-field fermion Green's function and the vertex matrix are given by

$$\mathcal{G}_{\mathbf{k}}(i\omega_m) = \frac{1}{(i\omega_m)^2 - E_{\mathbf{k}}^2} \begin{pmatrix} (i\omega_m + \xi_{\mathbf{k}}) & -\Delta_{\mathbf{k}}^p \\ -\Delta_{\mathbf{k}}^{p*} & (i\omega_m - \xi_{\mathbf{k}}) \end{pmatrix}, \\ \Phi_{\mathbf{q}}(iv_n) = \begin{pmatrix} 0 & \hat{\phi}_{\mathbf{q}}(iv_n) \Gamma^p(\mathbf{k}) \\ \hat{\phi}_{-\mathbf{q}}^*(-iv_n) \Gamma^{p*}(\mathbf{k}) & 0 \end{pmatrix}. \quad (16)$$

After some algebra,  $\mathcal{S}_2^p$  can be written in a compact form

$$\mathcal{S}_2^p = \frac{1}{2} \sum_{\mathbf{q}, n} \left( \hat{\phi}_{\mathbf{q}}^*(iv_n) \hat{\phi}_{-\mathbf{q}}(-iv_n) \right) M(\mathbf{q}, iv_n) \begin{pmatrix} \hat{\phi}_{\mathbf{q}}(iv_n) \\ \hat{\phi}_{-\mathbf{q}}^*(-iv_n) \end{pmatrix} \quad (17)$$

where the inverse boson propagator  $M(\mathbf{q}, iv_n)$  takes the form

$$M(\mathbf{q}, iv_n) = \begin{pmatrix} M_{11}(\mathbf{q}, iv_n) & M_{12}(\mathbf{q}, iv_n) \\ M_{21}(\mathbf{q}, iv_n) & M_{22}(\mathbf{q}, iv_n) \end{pmatrix}. \quad (18)$$

The matrix elements are given by

$$M_{11} = \frac{1}{4\lambda} + \frac{T}{2S} \sum_{\mathbf{k}, m} \mathcal{G}_{\mathbf{k}-\mathbf{q}/2}^{11}(i\omega_m) \mathcal{G}_{\mathbf{k}+\mathbf{q}/2}^{22}(i\omega_m + iv_n) |\Gamma^p(\mathbf{k})|^2, \\ M_{22} = \frac{1}{4\lambda} + \frac{T}{2S} \sum_{\mathbf{k}, m} \mathcal{G}_{\mathbf{k}-\mathbf{q}/2}^{22}(i\omega_m) \mathcal{G}_{\mathbf{k}+\mathbf{q}/2}^{11}(i\omega_m + iv_n) |\Gamma^p(\mathbf{k})|^2, \\ M_{12} = \frac{T}{2S} \sum_{\mathbf{k}, m} \mathcal{G}_{\mathbf{k}-\mathbf{q}/2}^{12}(i\omega_m) \mathcal{G}_{\mathbf{k}+\mathbf{q}/2}^{12}(i\omega_m + iv_n) [\Gamma^{p*}(\mathbf{k})]^2, \\ M_{21} = \frac{T}{2S} \sum_{\mathbf{k}, m} \mathcal{G}_{\mathbf{k}-\mathbf{q}/2}^{21}(i\omega_m) \mathcal{G}_{\mathbf{k}+\mathbf{q}/2}^{21}(i\omega_m + iv_n) [\Gamma^p(\mathbf{k})]^2. \quad (19)$$

It is easy to prove that these matrix elements satisfy

$$M_{11}^*(\mathbf{q}, iv_n) = M_{22}(\mathbf{q}, iv_n), \quad M_{12}^*(\mathbf{q}, iv_n) = M_{21}(\mathbf{q}, iv_n). \quad (20)$$

Completing the fermion Matsubara frequency summation, we obtain

$$M_{11} = \frac{1}{4\lambda} - \int \frac{d^2 \mathbf{k}}{(2\pi)^2} (u_1 + u_2) |\Gamma^p(\mathbf{k})|^2 \tanh \left( \frac{E_{\mathbf{k}-\mathbf{q}/2}}{2T} \right), \\ M_{22} = \frac{1}{4\lambda} - \int \frac{d^2 \mathbf{k}}{(2\pi)^2} (u_1^* + u_2^*) |\Gamma^p(\mathbf{k})|^2 \tanh \left( \frac{E_{\mathbf{k}-\mathbf{q}/2}}{2T} \right), \\ M_{12} = - \int \frac{d^2 \mathbf{k}}{(2\pi)^2} (v_1 + v_2) [\Gamma^{p*}(\mathbf{k})]^2 \tanh \left( \frac{E_{\mathbf{k}-\mathbf{q}/2}}{2T} \right), \\ M_{21} = - \int \frac{d^2 \mathbf{k}}{(2\pi)^2} (v_1^* + v_2^*) [\Gamma^p(\mathbf{k})]^2 \tanh \left( \frac{E_{\mathbf{k}-\mathbf{q}/2}}{2T} \right), \quad (21)$$

where the auxiliary functions are defined as

$$u_1 = \frac{E_{\mathbf{k}-\mathbf{q}/2} - \xi_{\mathbf{k}-\mathbf{q}/2}}{4E_{\mathbf{k}-\mathbf{q}/2}} \frac{iv_n + E_{\mathbf{k}-\mathbf{q}/2} + \xi_{\mathbf{k}+\mathbf{q}/2}}{(iv_n + E_{\mathbf{k}-\mathbf{q}/2})^2 - E_{\mathbf{k}+\mathbf{q}/2}^2}, \\ u_2 = - \frac{E_{\mathbf{k}-\mathbf{q}/2} + \xi_{\mathbf{k}-\mathbf{q}/2}}{4E_{\mathbf{k}-\mathbf{q}/2}} \frac{iv_n - E_{\mathbf{k}-\mathbf{q}/2} + \xi_{\mathbf{k}+\mathbf{q}/2}}{(iv_n - E_{\mathbf{k}-\mathbf{q}/2})^2 - E_{\mathbf{k}+\mathbf{q}/2}^2}, \\ v_1 = \frac{\Delta_{\mathbf{k}-\mathbf{q}/2}^p \Delta_{\mathbf{k}+\mathbf{q}/2}^p}{4E_{\mathbf{k}-\mathbf{q}/2} [(iv_n + E_{\mathbf{k}-\mathbf{q}/2})^2 - E_{\mathbf{k}+\mathbf{q}/2}^2]}, \\ v_2 = \frac{\Delta_{\mathbf{k}-\mathbf{q}/2}^p \Delta_{\mathbf{k}+\mathbf{q}/2}^p}{4E_{\mathbf{k}-\mathbf{q}/2} [(iv_n - E_{\mathbf{k}-\mathbf{q}/2})^2 - E_{\mathbf{k}+\mathbf{q}/2}^2]}. \quad (22)$$

It is more physical to decompose the fluctuation into its real and imaginary parts, i.e.,  $\hat{\phi}(x) = \sigma(x) + i\pi(x)$ . In momentum space we have  $\hat{\phi}_{\mathbf{q}}(iv_n) = \sigma_{\mathbf{q}}(iv_n) + i\pi_{\mathbf{q}}(iv_n)$  and  $\hat{\phi}_{\mathbf{q}}^*(iv_n) = \sigma_{\mathbf{q}}^*(iv_n) - i\pi_{\mathbf{q}}^*(iv_n) = \sigma_{-\mathbf{q}}(-iv_n) - i\pi_{-\mathbf{q}}(-iv_n)$ . Thus, the Gaussian fluctuation part of the effective action can be expressed as

$$\mathcal{S}_2^p = \frac{1}{2} \sum_{\mathbf{q}, n} \left( \sigma_{\mathbf{q}}^*(iv_n) \pi_{\mathbf{q}}^*(iv_n) \right) \Pi(\mathbf{q}, iv_n) \begin{pmatrix} \sigma_{\mathbf{q}}(iv_n) \\ \pi_{\mathbf{q}}(iv_n) \end{pmatrix}, \quad (23)$$

where the inverse boson propagator reads

$$\Pi = \begin{pmatrix} (M_{11} + M_{12} + M_{21} + M_{22}) & i(-M_{11} - M_{12} + M_{21} + M_{22}) \\ i(M_{11} - M_{12} + M_{21} - M_{22}) & (M_{11} - M_{12} - M_{21} + M_{22}) \end{pmatrix}. \quad (24)$$

The low-energy dynamics is governed by the gapless Goldstone mode. Diagonalizing the matrix  $\Pi$ , we obtain two eigenmodes. Their inverse propagators are given by

$$\mathcal{D}_{\theta/\eta}^{-1}(\mathbf{q}, iv_n) = M_{11} + M_{22} \mp \sqrt{(M_{11} - M_{22})^2 + 4M_{12}M_{21}}. \quad (25)$$

We can prove that  $\mathcal{D}_{\theta}^{-1}(\mathbf{0}, 0) = 0$ , which indicates that the  $\theta$ -mode is gapless, i.e., the Goldstone mode. It is a mixture of  $\sigma$  and  $\pi$  components and can be expressed as

$$\theta_{\mathbf{q}}(iv_n) = C \left[ \mathcal{D}_{\theta}^{-1}(\mathbf{q}, iv_n) \sigma_{\mathbf{q}}(iv_n) + \mathcal{D}_{\eta}^{-1}(\mathbf{q}, iv_n) \pi_{\mathbf{q}}(iv_n) \right], \quad (26)$$

where  $C$  is a normalization coefficient.

To study the low-energy dynamics, we make the low-energy expansion of  $M_{ij}$  ( $i, j = 1, 2$ ) to the quadratic order in frequency and momentum, the result is

$$M_{ij}(\mathbf{q}, iv_n) = A_{ij} + iv_n B_{ij} + (iv_n)^2 C_{ij} + D_{ij}^x q_x^2 + D_{ij}^y q_y^2. \quad (27)$$

The expansion coefficients can be evaluated as

$$A_{11} = A_{22} = \frac{1}{4\lambda} - \int \frac{d^2 \mathbf{k}}{(2\pi)^2} (E_{\mathbf{k}}^2 + \xi_{\mathbf{k}}^2) \frac{|\Gamma^p(\mathbf{k})|^2}{8E_{\mathbf{k}}^3} \tanh \left( \frac{E_{\mathbf{k}}}{2T} \right), \\ B_{11} = -B_{22} = - \int \frac{d^2 \mathbf{k}}{(2\pi)^2} \frac{\xi_{\mathbf{k}} |\Gamma^p(\mathbf{k})|^2}{8E_{\mathbf{k}}^3} \tanh \left( \frac{E_{\mathbf{k}}}{2T} \right), \\ C_{11} = C_{22} = - \int \frac{d^2 \mathbf{k}}{(2\pi)^2} (E_{\mathbf{k}}^2 + \xi_{\mathbf{k}}^2) \frac{|\Gamma^p(\mathbf{k})|^2}{32E_{\mathbf{k}}^5} \tanh \left( \frac{E_{\mathbf{k}}}{2T} \right), \\ A_{12} = A_{21} = \Delta^2 \int \frac{d^2 \mathbf{k}}{(2\pi)^2} \frac{|\Gamma^p(\mathbf{k})|^4}{8E_{\mathbf{k}}^3} \tanh \left( \frac{E_{\mathbf{k}}}{2T} \right), \\ B_{12} = B_{21} = 0, \\ C_{12} = C_{21} = \Delta^2 \int \frac{d^2 \mathbf{k}}{(2\pi)^2} \frac{|\Gamma^p(\mathbf{k})|^4}{32E_{\mathbf{k}}^5} \tanh \left( \frac{E_{\mathbf{k}}}{2T} \right). \quad (28)$$

The coefficients  $D_{ij}$  can be obtained (see the Appendix. A) but quite lengthy. Here we show the combined quantities  $\rho_i^p = 4m\Delta^2(D_{11}^i + D_{22}^i - D_{12}^i - D_{21}^i)$  ( $i = x, y$ ), which are exactly the superfluid density along the  $x$  and  $y$  directions. After a lengthy calculation we obtain

$$\rho_i^p = \int \frac{d^2\mathbf{k}}{(2\pi)^2} \left[ n_0(\mathbf{k}) - \frac{k_i^2}{4mT} \operatorname{sech}^2\left(\frac{E_{\mathbf{k}}}{2T}\right) \right]. \quad (29)$$

At zero temperature, the superfluid density is isotropic for both  $p_x$  and  $p_x + ip_y$  pairings and we have  $\rho_x^p = \rho_y^p = n$  as required by the Galilean invariance [31]. However, for  $p_x$  pairing, finite temperature effect generates anisotropy of the superfluid density. Finally, the low-energy behavior of the  $\theta$ -mode or the Goldstone mode is given by

$$\mathcal{D}_{\theta}^{-1} = -\zeta^p (iv_n)^2 + \frac{1}{4m\Delta^2} (\rho_x^p q_x^2 + \rho_y^p q_y^2), \quad (30)$$

where  $\zeta^p = \zeta_0^p + B_{11}^2/A_{12}$  with  $\zeta_0^p = -2(C_{11} - C_{12})$ . The Goldstone mode velocity or sound velocity reads

$$v_i^p = \sqrt{\frac{\rho_i^p}{4m\Delta^2\zeta^p}}. \quad (31)$$

In this low-energy approximation, the contribution of the Goldstone mode to the thermodynamic potential can be given by [49]

$$\Omega_2^p = \int \frac{d^2\mathbf{q}}{(2\pi)^2} T \ln\left(1 - e^{-\varepsilon_{\mathbf{q}}/T}\right) = -\frac{\zeta(3)T^3}{2\pi(v_x^p v_y^p)}, \quad (32)$$

where the dispersion relation of the Goldstone mode is given by  $\varepsilon_{\mathbf{q}} = [\sum_{i=x,y} (v_i^p q_i)^2]^{1/2}$  and  $\zeta(x)$  is the Riemann zeta function. At finite temperature, we take into account the fluctuation contribution to the number density. The total fermion density  $n$  can be given by

$$n = n_0 - \frac{\partial \Omega_2^p}{\partial \mu} = n_0 - \frac{\zeta(3)T^3}{2\pi(v_x^p v_y^p)^2} \frac{\partial(v_x^p v_y^p)}{\partial \mu}. \quad (33)$$

At  $T = 0$  we have  $n = n_0$  and therefore the quantum fluctuations [50–52] are not taken into account in the present theory. For  $s$ -wave pairing, it was found that inclusion of quantum fluctuations leads to slight correction to the KT transition [53, 54]. Thus we expect that the present theory can provides reliable results for the KT and VAL transition for higher partial wave pairings.

## B. Kosterlitz-Thouless and vortex-antivortex lattice melting transitions

The KT and VAL melting temperatures are both directly related to the stiffness  $J_i = \rho_i^p/(4m)$  [33–35, 49]:

$$T_{\text{KT}} = \frac{\pi}{2} \sqrt{J_x^p(T_{\text{KT}}) J_y^p(T_{\text{KT}})}, \quad T_{\text{M}} = 0.3 \sqrt{J_x^p(T_{\text{M}}) J_y^p(T_{\text{M}})}. \quad (34)$$

For the anisotropic  $p_x$  pairing, the vortex might be elliptically shaped and the usual square vortex-antivortex lattice will also

deform accordingly just like the case with anisotropic spin-orbit coupling [55]. However, one can scale one direction so that the scaled vortex is circular (the scaled lattice thus becomes square); thus we can apply Eq. (34) to the scaled vortex and lattice. Then for a given  $E_b$  and number density, the gap equation Eq.(12), number density equation Eq.(33), and critical temperature equations Eq.(34) can be solved self-consistently to give  $T_{\text{KT}}$ ,  $T_{\text{M}}$  and  $\Delta$  and  $\mu$  at  $T_{\text{KT}}$  or  $T_{\text{M}}$ .

The numerical results are shown in Fig.1 in which we plot the transition temperatures  $T_{\text{KT}}$  and  $T_{\text{M}}$ , the chemical potential, the order parameter, and the sound velocity at  $T_{\text{KT}}$  and  $T_{\text{M}}$  as functions of  $E_b$ . The  $E_b$  dependence of  $T_{\text{KT}}$  clearly shows the BCS-BEC crossover when  $E_b$  is tuned from positive to negative values (Note that for  $p$ -wave pairing in 2D, an attractive potential does not necessarily lead to a bound state; when  $E_b > 0$  the two-fermion state is a scattering state.). The chemical potential at  $T_{\text{KT}}$  and  $T_{\text{M}}$  are almost the same for a given  $p$ -wave pairings; similarly, the order parameter at  $T_{\text{KT}}$  and  $T_{\text{M}}$  are also almost the same. In the deep BEC region where  $E_b < 0$  with a large magnitude, the transition temperatures  $T_{\text{KT}}$  and  $T_{\text{M}}$  are found to be constants  $T_{\text{KT}} \simeq 0.0625\epsilon_F$  and  $T_{\text{M}} \simeq (0.6/\pi)T_{\text{KT}}$  which are comparable to the  $s$ -wave pairing case [49] if one takes the current relation  $n = (k_F^2/4\pi)$  into account. Besides, the anisotropy in the sound velocity disappears for  $p_x$  pairing in deep BEC region as illuminated in the plot of the sound velocities  $v_x$  and  $v_y$ , because the basic degrees of freedom are compactly bound bosons now and the Yoshida term in Eq. (29) is suppressed.

We note here that, in all the curves especially for those associate KT transitions, there are non-analytic behavior at the BCS-BEC crossover point  $\mu = 0$ . To illuminate this more explicitly, we show the results for  $T_{\text{KT}}$  around the region  $\mu \sim 0$  in the inserted figure for the anisotropic  $p_x$  pairing, which is more obvious than the isotropic  $p_x + ip_y$  pairing. In order to understand the non-analyticity, let's explore the property of the most relevant quantity  $\zeta_0^p$  around  $\mu = 0$ . The first two derivatives of  $\zeta_0^p$  with respect to  $\mu$  are given by

$$\frac{\partial \zeta_0^p}{\partial \mu} = \frac{1}{S} \sum_{\mathbf{k}} \frac{\xi_{\mathbf{k}} |\Gamma^p(\mathbf{k})|^2}{8E_{\mathbf{k}}^4} \left[ \frac{3 \tanh\left(\frac{E_{\mathbf{k}}}{2T}\right)}{E_{\mathbf{k}}} - \frac{\operatorname{sech}^2\left(\frac{E_{\mathbf{k}}}{2T}\right)}{2T} \right], \quad (35)$$

$$\frac{\partial^2 \zeta_0^p}{\partial \mu^2} = \frac{1}{S} \sum_{\mathbf{k}} |\Gamma^p(\mathbf{k})|^2 \left[ \frac{3(5\xi_{\mathbf{k}}^2 - E_{\mathbf{k}}^2)}{8E_{\mathbf{k}}^7} \tanh\left(\frac{E_{\mathbf{k}}}{2T}\right) - \frac{|\Delta_{\mathbf{k}}^p|^2}{16TE_{\mathbf{k}}^6} \times \right. \\ \left. \operatorname{sech}^2\left(\frac{E_{\mathbf{k}}}{2T}\right) - \frac{\xi_{\mathbf{k}}^2}{16T^2E_{\mathbf{k}}^5} \tanh\left(\frac{E_{\mathbf{k}}}{2T}\right) \operatorname{sech}^2\left(\frac{E_{\mathbf{k}}}{2T}\right) \right]. \quad (36)$$

For small  $\mu \rightarrow 0^+$ ,  $\partial \zeta_0^p / \partial \mu$  is finite but

$$\frac{\partial^2 \zeta_0^p}{\partial \mu^2} \sim \frac{1}{T\Delta^4} \ln \frac{\mu}{\Delta}. \quad (37)$$

As  $\zeta_0^p$  appears in  $n$  and  $\rho_i^p$ , this shows that the higher order derivatives of  $n$  and  $\rho_i^p$  with respect to  $\mu$  is not analytic at the point where  $\mu = 0$ . Also,  $T_{\text{KT}}$ ,  $T_{\text{M}}$ , and sound velocity  $v$  are all non-analytic at the point where  $\mu = 0$ . But we note that the temperature effect weakens the non-analyticities as can be seen from the above equation. Thus, the BCS-BEC evolution in  $p$ -wave pairing system is a actually a phase transition

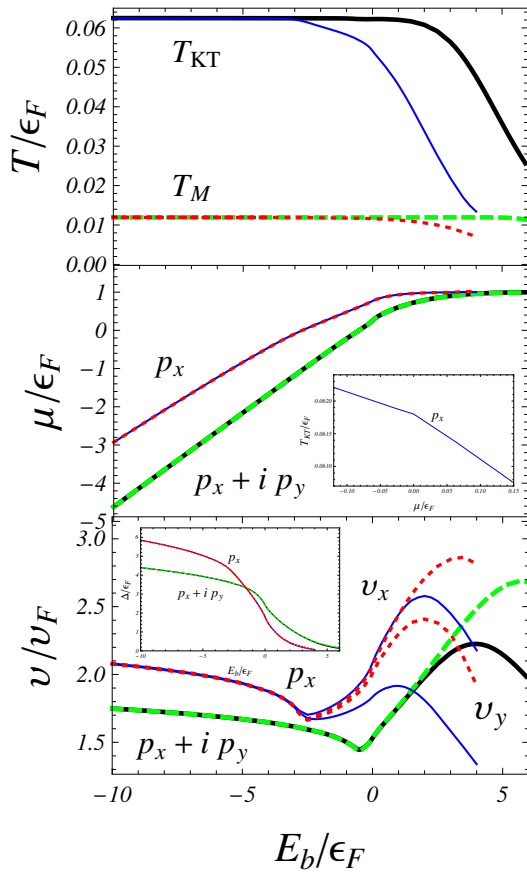


FIG. 1: (Color online) Upper panel: the transition temperatures,  $T_{KT}$  (solid lines) and  $T_M$  (dashed lines) as functions of the two-body binding energy  $E_b$  for both the isotropic  $p_x + ip_y$  pairing (black and green thick lines) and anisotropic  $p_x$  pairing (blue and red thin lines). Lower panels: the chemical potential  $\mu$  and sound velocity  $v$  as functions of  $E_b$  at  $T_{KT}$  and  $T_M$ , where two anisotropic velocities  $v_x$  and  $v_y$  are shown for the anisotropic  $p_x$  pairing. The inserts are the zoom-in plot of  $T_{KT}$  with respect to  $\mu$  around the BCS-BEC transition point  $\mu = 0$  for the anisotropic  $p_x$  pairing and the order parameter  $\Delta$ , respectively. Here, the parameters for NSR potential are chosen to be  $k_0 = 10^{3/2}k_F$  and  $k_1 = 10^{1/2}k_F$  with  $k_F$  and  $\epsilon_F$  Fermi momentum and energy, respectively.

although there is no further symmetry broken during this process.

The sound velocities behave non-monotonically versus  $E_b$  which we'd like to analyze in more detail. For the anisotropic  $p_x$  pairing, the sound velocities along  $x$  and  $y$  directions split in the BCS region ( $E_b > 0$  and is large) and merge into one single curve in the deep BEC region. For the isotropic  $p_x + ip_y$  pairing, we plot the relevant functions  $\zeta_0^p$ ,  $\zeta^p$  and  $\rho^p$  versus the chemical potential  $\mu$  in Fig.2 to understand the extrema in the sound velocities. As can be seen, the term  $B_{11}^2/A_{12}$  dominates  $\zeta^p$  at low temperature which indicates the importance of the  $\sigma$

component in  $\theta$  mode and the increasing feature of the sound velocities in the BCS region is due to the fast decreasing of  $\zeta^p$ . The decreasing feature of the sound velocity for even larger  $E_b$  is mainly due to pair breaking effect in the two-body scattering state region which will become significant when  $\Delta$  is small.

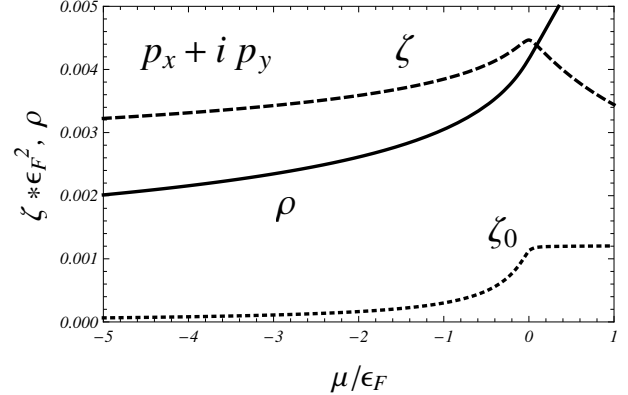


FIG. 2: An illumination of the functions  $\zeta_0^p$ ,  $\zeta^p$  and  $\rho^p$  involved in the sound velocity  $v$  with the chemical potential  $\mu$  at fixed temperature  $T = 0.06\epsilon_F$  and order parameter  $\Delta = 4\epsilon_F$  which are approximately the values at the BEC-side Kosterlitz-Thouless transition with isotropic  $p_x + ip_y$  pairing. The parameters are the same as in Fig. 1.

### III. *d*-WAVE PAIRING IN SPIN-1/2 FERMI GASES

#### A. Formalism in Gaussian approximation

For *d*-wave pairing, Fermi surface mismatch might be introduced between different spin components through Zeeman effect induced by a magnetic field [56–59] or through spin-orbit coupling [60]. The Hamiltonian density can be written as [20]

$$\mathcal{H} = \sum_{\mathbf{k}, s=\uparrow\downarrow} \psi_{\mathbf{k}, s}^\dagger \xi_{\mathbf{k}, s} \psi_{\mathbf{k}, s} + \sum_{\mathbf{k}, \mathbf{k}', \mathbf{q}} V_{\mathbf{k}\mathbf{k}'}^d b_{\mathbf{k}\mathbf{q}}^\dagger b_{\mathbf{k}'\mathbf{q}}, \quad (38)$$

where  $\psi_{\mathbf{k}, s}$  represents the fermion annihilation operator with spin  $s = \pm 1$ ,  $b_{\mathbf{k}\mathbf{q}} = \psi_{-\mathbf{k}+\mathbf{q}/2, \downarrow} \psi_{\mathbf{k}+\mathbf{q}/2, \uparrow}$  and  $\xi_{\mathbf{k}, s} = \xi_{\mathbf{k}} - s\delta\mu$ . Here and in the following, when  $s$  appears in the calculation, the correspondence  $\uparrow$  ( $\downarrow$ )  $\leftrightarrow$   $+$  ( $-$ ) should be understood. For the sake of simplicity, we consider a separable *d*-wave interaction potential [25]:

$$V_{\mathbf{k}\mathbf{k}'}^d = -\lambda \Gamma^d(\mathbf{k}) \Gamma^{d*}(\mathbf{k}'), \quad (39)$$

where  $\lambda$  is the interaction strength. The gamma functions are defined according to NSR-type potentials [19]:

$$\Gamma_s^d(\mathbf{k}) = \frac{(k_x + ik_y)^2/k_1^2}{(1 + k/k_0)^{5/2}}, \quad \Gamma_a^d(\mathbf{k}) = \frac{(k_x^2 - k_y^2)/k_1^2}{(1 + k/k_0)^{5/2}} \quad (40)$$

with  $k = |\mathbf{k}|$  and  $s$  and  $a$  representing the symmetric (or isotropic)  $d_{x^2-y^2} + 2id_{xy}$  and asymmetric (or anisotropic)  $d_{x^2-y^2}$  pairings, respectively. The form of the denominator is chosen

to mimic the amplitude damping for  $d$ -wave partial potential at large momentum [19].

Then, the partition function at finite temperature is given by

$$\mathcal{Z} = \int \prod_{s=\uparrow\downarrow} [d\psi_s^\dagger] [d\psi_s] \exp \left\{ - \int_0^\beta d\tau \left( \sum_{\mathbf{k},s=\uparrow\downarrow} \psi_{\mathbf{k},s}^\dagger \partial_\tau \psi_{\mathbf{k},s} + \mathcal{H} \right) \right\}, \quad (41)$$

where  $\tau = it$  is the imaginary time and  $\beta = 1/T$  with  $T$  being the temperature. Introducing the auxiliary field  $\phi_{\mathbf{q}}(\tau) = \lambda \sum_{\mathbf{k}} \Gamma^d(\mathbf{k}) b_{\mathbf{k}\mathbf{q}}$  through Hubbard-Stratonovich transformation, the partition function can be rewritten as:

$$\begin{aligned} \mathcal{Z} = & \int [d\phi^*] [d\phi] [d\Psi^\dagger] [d\Psi] \exp \left\{ - \int_0^\beta d\tau \left[ \sum_{\mathbf{k}} \frac{|\phi_{\mathbf{k}}(\tau)|^2}{\lambda} \right. \right. \\ & \left. \left. + \sum_{\mathbf{k},\mathbf{k}'} \left( \xi_{\mathbf{k}} \delta_{\mathbf{k},\mathbf{k}'} + \Psi_{\mathbf{k}}^\dagger G_{\mathbf{k},\mathbf{k}'}^{-1}(\tau) \Psi_{\mathbf{k}'} \right) \right] \right\}, \end{aligned} \quad (42)$$

where the fermion field in Nambu-Gor'kov space is  $\Psi_{\mathbf{k}}^\dagger = (\psi_{\mathbf{k},\uparrow}^\dagger, \psi_{-\mathbf{k},\downarrow})$ . The inverse propagator is then a  $2 \times 2$  matrix which is given by

$$G_{\mathbf{k},\mathbf{k}'}^{-1}(\tau) = \begin{pmatrix} (\partial_\tau + \xi_{\mathbf{k}\uparrow}) \delta_{\mathbf{k},\mathbf{k}'} & -\phi_{\mathbf{k}-\mathbf{k}'}(\tau) \Gamma^d(\frac{\mathbf{k}+\mathbf{k}'}{2}) \\ -\phi_{-\mathbf{k}+\mathbf{k}'}^*(\tau) \Gamma^{d*}(\frac{\mathbf{k}+\mathbf{k}'}{2}) & (\partial_\tau - \xi_{\mathbf{k}\downarrow}) \delta_{\mathbf{k},\mathbf{k}'} \end{pmatrix}. \quad (43)$$

Integrating out the fermion degrees of freedom, we can get a bosonic version of partition function

$$\mathcal{Z} = \int [d\phi^*] [d\phi] e^{-S_{\text{eff}}^d[\phi^*, \phi]}, \quad (44)$$

with the effective action

$$S_{\text{eff}}^d = \int_0^\beta d\tau \left[ \sum_{\mathbf{k}} \frac{|\phi_{\mathbf{k}}(\tau)|^2}{\lambda} + \sum_{\mathbf{k},\mathbf{k}'} \left( \xi_{\mathbf{k}} \delta_{\mathbf{k},\mathbf{k}'} - \text{Tr} \ln G_{\mathbf{k},\mathbf{k}'}^{-1}(\tau) \right) \right], \quad (45)$$

where the trace is taken over imaginary time, momentum and Nambu-Gorkov spaces.

To proceed, we decompose the auxiliary field  $\phi_{\mathbf{q}}(\tau)$  into its mean-field and fluctuation parts,

$$\phi_{\mathbf{q}}(\tau) = \Delta_{\mathbf{q},0} + \hat{\phi}_{\mathbf{q}}(\tau). \quad (46)$$

The effective action can be evaluated in powers of the fluctuation  $\hat{\phi}_{\mathbf{q}}(\tau)$ , i.e.,  $S_{\text{eff}}^d = S_0^d + S_2^d + \dots$ . Here we omit the linear term in the fluctuation since it vanishes due to the gap equation. The leading-order term  $S_0^d$  represents the mean-field contribution. The next-to-leading-order term  $S_2^d$ , which is quadratic in the fluctuation, represents the Gaussian fluctuations and hence the collective mode dynamics.

### 1. Mean field approximation

The mean-field effective potential can be obtained in a way parallel to the  $p$ -wave pairing case. We just write down the result:

$$\begin{aligned} S_0^d(\Delta) = & \beta S \left[ \frac{\Delta^2}{\lambda} + \int \frac{d^2\mathbf{k}}{(2\pi)^2} \xi_{\mathbf{k}} - \frac{T}{2} \sum_n \int \frac{d^2\mathbf{k}}{(2\pi)^2} \ln \text{Det} \mathcal{G}_{\mathbf{k}}^{-1}(i\omega_n) \right] \\ = & \beta S \left\{ \frac{\Delta^2}{\lambda} - \int \frac{d^2\mathbf{k}}{(2\pi)^2} \left[ E_{\mathbf{k}} - \xi_{\mathbf{k}} + \sum_s T \ln \left( 1 + e^{-\frac{E_{\mathbf{k}} + s\delta\mu}{T}} \right) \right] \right\}, \end{aligned} \quad (47)$$

where the excitation energy is  $E_{\mathbf{k}} = (\xi_{\mathbf{k}}^2 + |\Delta_{\mathbf{k}}^d|^2)^{1/2}$  with the pairing energy  $\Delta_{\mathbf{k}}^d = \Delta \Gamma^d(\mathbf{k})$  and the inverse fermion propagator in energy-momentum space is in the following form:

$$\mathcal{G}_{\mathbf{k}}^{-1}(i\omega_m) = \begin{pmatrix} (i\omega_m + \xi_{\mathbf{k}\uparrow}) & -\Delta_{\mathbf{k}}^d \\ -\Delta_{\mathbf{k}}^{d*} & (i\omega_m - \xi_{\mathbf{k}\downarrow}) \end{pmatrix}. \quad (48)$$

The gap equation for order parameter  $\Delta$  can be obtained by the saddle point condition  $\partial S_0^d(\Delta)/\partial\Delta = 0$ :

$$\frac{2}{\lambda} = \sum_{s=\pm} \int \frac{d^2\mathbf{k}}{(2\pi)^2} \frac{|\Gamma^d(\mathbf{k})|^2}{2E_{\mathbf{k}}} \tanh \left( \frac{E_{\mathbf{k}} + s\delta\mu}{2T} \right). \quad (49)$$

The number density can be obtained through the thermodynamic relation  $n = -\partial\Omega/\partial\mu = -(\partial S_{\text{eff}}^d(\Delta)/\partial\mu)/\beta S$  as:

$$\begin{aligned} n_0 & \equiv \sum_{s=\pm} \int \frac{d^2\mathbf{k}}{(2\pi)^2} n_0(\mathbf{k}, s) \\ & = \frac{1}{2} \sum_{s=\pm} \int \frac{d^2\mathbf{k}}{(2\pi)^2} \left[ 1 - \frac{\xi_{\mathbf{k}}}{E_{\mathbf{k}}} \tanh \left( \frac{E_{\mathbf{k}} + s\delta\mu}{2T} \right) \right]. \end{aligned} \quad (50)$$

Similar to the  $p$ -wave pairings, the interaction strength  $\lambda$  can be physically characterized by the two-body binding energy  $E_b$  in vacuum [19]:

$$\frac{1}{\lambda} = \int \frac{d^2\mathbf{k}}{(2\pi)^2} \frac{|\Gamma^d(\mathbf{k})|^2}{2\epsilon_{\mathbf{k}} - E_b}. \quad (51)$$

Still, the weak and strong attraction limits correspond to  $E_b \rightarrow +\infty$  and  $E_b \rightarrow -\infty$ , respectively.

### 2. Gaussian fluctuation and Goldstone mode

Similar to the  $p$ -wave pairing case, the contribution of Gaussian fluctuation to the effective action can be evaluated as

$$\begin{aligned} S_2^d = & \sum_{\mathbf{q},n} \left\{ \frac{|\hat{\phi}_{\mathbf{q}}(i\nu_n)|^2}{\lambda} + \frac{T}{2S} \sum_{\mathbf{k},m} \text{tr} \left[ \mathcal{G}_{\mathbf{k}-\mathbf{q}/2}(i\omega_m) \right. \right. \\ & \left. \left. \times \Phi_{-\mathbf{q}}(-i\nu_n) \mathcal{G}_{\mathbf{k}+\mathbf{q}/2}(i\omega_m + i\nu_n) \Phi_{\mathbf{q}}(i\nu_n) \right] \right\}, \end{aligned} \quad (52)$$

where  $\nu_n = 2\pi n T$  ( $n \in \mathbb{Z}$ ) is the boson Matsubara frequency and the fermion propagator and the collective mode matrix are in the following forms:

$$\begin{aligned} \mathcal{G}_{\mathbf{k}}(i\omega_n) & = \frac{1}{(i\omega_n - \delta\mu)^2 - E_{\mathbf{k}}^2} \begin{pmatrix} (i\omega_n - \xi_{\mathbf{k}\downarrow}) & \Delta_{\mathbf{k}}^d \\ \Delta_{\mathbf{k}}^{d*} & (i\omega_n + \xi_{\mathbf{k}\uparrow}) \end{pmatrix}, \\ \Phi_{\mathbf{q}}(i\nu_n) & = \begin{pmatrix} 0 & -\hat{\phi}_{\mathbf{q}}(i\nu_n) \Gamma^d(\mathbf{k}) \\ -\hat{\phi}_{-\mathbf{q}}^*(-i\nu_n) \Gamma^{d*}(\mathbf{k}) & 0 \end{pmatrix}. \end{aligned} \quad (53)$$

After some algebra,  $S_2^d$  can be written in a compact form

$$S_2^d = \frac{1}{2} \sum_{\mathbf{q},n} \left( \hat{\phi}_{\mathbf{q}}^*(i\nu_n) \hat{\phi}_{-\mathbf{q}}(-i\nu_n) \right) M(\mathbf{q}, i\nu_n) \begin{pmatrix} \hat{\phi}_{\mathbf{q}}(i\nu_n) \\ \hat{\phi}_{-\mathbf{q}}^*(-i\nu_n) \end{pmatrix} \quad (54)$$

where the inverse boson propagator  $M(\mathbf{q}, iv_n)$  takes the form

$$M(\mathbf{q}, iv_n) = \begin{pmatrix} M_{11}(\mathbf{q}, iv_n) & M_{12}(\mathbf{q}, iv_n) \\ M_{21}(\mathbf{q}, iv_n) & M_{22}(\mathbf{q}, iv_n) \end{pmatrix}. \quad (55)$$

The matrix elements of  $M$  are related to the matrix elements of fermion propagator  $\tilde{G}_{\mathbf{k}}(i\omega_m)$  as

$$\begin{aligned} M_{11} &= \frac{1}{\lambda} + \frac{T}{S} \sum_{\mathbf{k}, m} \mathcal{G}_{\mathbf{k}-\mathbf{q}/2}^{11}(i\omega_m) \mathcal{G}_{\mathbf{k}+\mathbf{q}/2}^{22}(i\omega_m + iv_n) |\Gamma^d(\mathbf{k})|^2, \\ M_{22} &= \frac{1}{\lambda} + \frac{T}{S} \sum_{\mathbf{k}, m} \mathcal{G}_{\mathbf{k}-\mathbf{q}/2}^{22}(i\omega_m) \mathcal{G}_{\mathbf{k}+\mathbf{q}/2}^{11}(i\omega_m + iv_n) |\Gamma^d(\mathbf{k})|^2, \\ M_{12} &= \frac{T}{S} \sum_{\mathbf{k}, m} \mathcal{G}_{\mathbf{k}-\mathbf{q}/2}^{12}(i\omega_m) \mathcal{G}_{\mathbf{k}+\mathbf{q}/2}^{12}(i\omega_m + iv_n) (\Gamma^{d*}(\mathbf{k}))^2, \\ M_{21} &= \frac{T}{S} \sum_{\mathbf{k}, m} \mathcal{G}_{\mathbf{k}-\mathbf{q}/2}^{21}(i\omega_m) \mathcal{G}_{\mathbf{k}+\mathbf{q}/2}^{21}(i\omega_m + iv_n) (\Gamma^d(\mathbf{k}))^2. \end{aligned} \quad (56)$$

It is easy to prove that these matrix elements satisfy

$$M_{11}^*(\mathbf{q}, iv_n) = M_{22}(\mathbf{q}, iv_n), \quad M_{12}^*(\mathbf{q}, iv_n) = M_{21}(\mathbf{q}, iv_n). \quad (57)$$

Now, we complete the summation over fermion Matsubara frequency  $i\omega_m$  and find

$$\begin{aligned} M_{11} &= \frac{1}{\lambda} - \frac{1}{S} \sum_{\mathbf{k}, s=\pm} (u_1 + u_2) |\Gamma^d(\mathbf{k})|^2 \tanh\left(\frac{E_{\mathbf{k}-\mathbf{q}/2} + s\delta\mu}{2T}\right), \\ M_{22} &= \frac{1}{\lambda} - \frac{1}{S} \sum_{\mathbf{k}, s=\pm} (u_1^* + u_2^*) |\Gamma^d(\mathbf{k})|^2 \tanh\left(\frac{E_{\mathbf{k}-\mathbf{q}/2} + s\delta\mu}{2T}\right), \\ M_{12} &= -\frac{1}{S} \sum_{\mathbf{k}, s=\pm} (v_1 + v_2) (\Gamma^{d*}(\mathbf{k}))^2 \tanh\left(\frac{E_{\mathbf{k}-\mathbf{q}/2} + s\delta\mu}{2T}\right), \\ M_{21} &= -\frac{1}{S} \sum_{\mathbf{k}, s=\pm} (v_1^* + v_2^*) (\Gamma^d(\mathbf{k}))^2 \tanh\left(\frac{E_{\mathbf{k}-\mathbf{q}/2} + s\delta\mu}{2T}\right), \end{aligned} \quad (58)$$

where the auxiliary functions are defined as:

$$\begin{aligned} u_1(\mathbf{k}, \mathbf{q}, iv_n) &= \frac{E_{\mathbf{k}-\mathbf{q}/2} - \xi_{\mathbf{k}-\mathbf{q}/2}}{4E_{\mathbf{k}-\mathbf{q}/2}} \frac{iv_n + E_{\mathbf{k}-\mathbf{q}/2} + \xi_{\mathbf{k}+\mathbf{q}/2}}{(iv_n + E_{\mathbf{k}-\mathbf{q}/2})^2 - E_{\mathbf{k}+\mathbf{q}/2}^2}, \\ u_2(\mathbf{k}, \mathbf{q}, iv_n) &= \frac{-E_{\mathbf{k}-\mathbf{q}/2} - \xi_{\mathbf{k}-\mathbf{q}/2}}{4E_{\mathbf{k}-\mathbf{q}/2}} \frac{iv_n - E_{\mathbf{k}-\mathbf{q}/2} + \xi_{\mathbf{k}+\mathbf{q}/2}}{(iv_n - E_{\mathbf{k}-\mathbf{q}/2})^2 - E_{\mathbf{k}+\mathbf{q}/2}^2}, \\ v_1(\mathbf{k}, \mathbf{q}, iv_n) &= \frac{\Delta_{\mathbf{k}-\mathbf{q}/2}^d \Delta_{\mathbf{k}+\mathbf{q}/2}^d}{4E_{\mathbf{k}-\mathbf{q}/2}[(iv_n + E_{\mathbf{k}-\mathbf{q}/2})^2 - E_{\mathbf{k}+\mathbf{q}/2}^2]}, \\ v_2(\mathbf{k}, \mathbf{q}, iv_n) &= \frac{\Delta_{\mathbf{k}-\mathbf{q}/2}^d \Delta_{\mathbf{k}+\mathbf{q}/2}^d}{4E_{\mathbf{k}-\mathbf{q}/2}[(iv_n - E_{\mathbf{k}-\mathbf{q}/2})^2 - E_{\mathbf{k}+\mathbf{q}/2}^2]}. \end{aligned} \quad (59)$$

It is more physical to decompose the collective mode  $\hat{\phi}(x)$  into a sum of real and imaginary parts, that is,  $\hat{\phi}(x) = \sigma(x) + i\pi(x)$ . Then Gaussian fluctuation part of the effective action can be reexpressed as

$$S_2^d = \frac{1}{2} \sum_{\mathbf{q}, n} \left( \begin{array}{cc} \sigma_{\mathbf{q}}^*(iv_n) & \pi_{\mathbf{q}}^*(iv_n) \end{array} \right) \Pi(\mathbf{q}, iv_n) \left( \begin{array}{c} \sigma_{\mathbf{q}}(iv_n) \\ \pi_{\mathbf{q}}(iv_n) \end{array} \right), \quad (60)$$

where the effective inverse boson propagator is

$$\Pi = \begin{pmatrix} (M_{11} + M_{12} + M_{21} + M_{22}) & i(-M_{11} - M_{12} + M_{21} + M_{22}) \\ i(M_{11} - M_{12} + M_{21} - M_{22}) & (M_{11} - M_{12} - M_{21} + M_{22}) \end{pmatrix}. \quad (61)$$

Thus, all the matrix elements of  $\Pi$  are real and the propagators of independent collective modes can be obtained through the diagonalization and we find

$$\mathcal{D}_{\theta/\eta}^{-1}(\mathbf{q}, iv_n) = M_{11} + M_{22} \mp \sqrt{(M_{11} - M_{22})^2 + 4M_{12}M_{21}}. \quad (62)$$

It can be verified that  $\mathcal{D}_\theta^{-1}(0, 0) = 0$  which shows  $\theta$  to be the Goldstone mode with the following mixing of  $\sigma$  and  $\pi$  components:

$$\theta_{\mathbf{q}}(iv_n) = C \left[ \mathcal{D}_\theta^{-1}(\mathbf{q}, iv_n) \sigma_{\mathbf{q}}(iv_n) + \mathcal{D}_\eta^{-1}(\mathbf{q}, iv_n) \pi_{\mathbf{q}}(iv_n) \right], \quad (63)$$

where  $C$  is a real normalization coefficient.

To study the low-energy dynamics, we make the low-energy expansion of  $M_{ij}$  ( $i, j = 1, 2$ ) to the quadratic order in frequency and momentum, the result is

$$M_{ij}(\mathbf{q}, iv_n) = A_{ij} + B_{ij}(iv_n) + C_{ij}(iv_n)^2 + D_{ij}^x q_x^2 + D_{ij}^y q_y^2, \quad (64)$$

with the coefficients

$$\begin{aligned} A_{11} = A_{22} &= \frac{1}{\lambda} - \frac{1}{S} \sum_{\mathbf{k}, s=\pm} (E_{\mathbf{k}}^2 + \xi_{\mathbf{k}}^2) \frac{|\Gamma^d(\mathbf{k})|^2}{8E_{\mathbf{k}}^3} \tanh\left(\frac{E_{\mathbf{k}} + s\delta\mu}{2T}\right), \\ B_{11} = -B_{22} &= -\frac{1}{S} \sum_{\mathbf{k}, s=\pm} \frac{\xi_{\mathbf{k}} |\Gamma^d(\mathbf{k})|^2}{8E_{\mathbf{k}}^3} \tanh\left(\frac{E_{\mathbf{k}} + s\delta\mu}{2T}\right), \\ C_{11} = C_{22} &= -\frac{1}{S} \sum_{\mathbf{k}, s=\pm} (E_{\mathbf{k}}^2 + \xi_{\mathbf{k}}^2) \frac{|\Gamma^d(\mathbf{k})|^2}{32E_{\mathbf{k}}^5} \tanh\left(\frac{E_{\mathbf{k}} + s\delta\mu}{2T}\right), \\ A_{12} = A_{21} &= \frac{1}{S} \sum_{\mathbf{k}, s=\pm} \frac{|\Delta_{\mathbf{k}}^d|^2 |\Gamma^d(\mathbf{k})|^2}{8E_{\mathbf{k}}^3} \tanh\left(\frac{E_{\mathbf{k}} + s\delta\mu}{2T}\right), \\ B_{12} = B_{21} &= 0, \\ C_{12} = C_{21} &= \frac{1}{S} \sum_{\mathbf{k}, s=\pm} \frac{|\Delta_{\mathbf{k}}^d|^2 |\Gamma^d(\mathbf{k})|^2}{32E_{\mathbf{k}}^5} \tanh\left(\frac{E_{\mathbf{k}} + s\delta\mu}{2T}\right). \end{aligned} \quad (65)$$

The coefficients  $D_{ij}$  is obtained together with  $p$ -wave pairing in the Appendix. A. Here we show the combined quantities  $\rho_i^d = 4m\Delta^2(D_{11}^i + D_{22}^i - D_{12}^i - D_{21}^i)$  ( $i = x, y$ ), which are exactly the superfluid density along the  $x$  and  $y$  directions. After a lengthy calculation we obtain

$$\rho_i^d = \sum_{s=\pm} \int \frac{d^2 \mathbf{k}}{(2\pi)^2} \left[ n_0(\mathbf{k}, s) - \frac{k_i^2}{4mT} \operatorname{sech}^2\left(\frac{E_{\mathbf{k}} + s\delta\mu}{2T}\right) \right]. \quad (66)$$

Compared to  $p$ -wave pairing, the superfluid density is isotropic for both  $d_{x^2-y^2} + 2id_{xy}$  and  $d_{x^2-y^2}$  pairings at any temperature which of course is consistent with the Galilean invariance [31]. Finally, the low-energy behavior of the  $\theta$ -mode or the Goldstone mode can be given by

$$\mathcal{D}_\theta^{-1} = -\zeta^d(iv_n)^2 + \frac{1}{4m\Delta^2} \rho^d \mathbf{q}^2, \quad (67)$$

where  $\zeta^d = \zeta_0^d + B_{11}^2/A_{12}$  with  $\zeta_0^d = -2(C_{11} - C_{12})$ . The sound velocity can be directly evaluated from this equation as

$$v^d = \sqrt{\frac{\rho^d}{4m\Delta^2\zeta^d}}. \quad (68)$$

Then, the thermodynamic potential owing to the contribution of Goldstone mode can be given by [49]

$$\Omega_2^d = \int \frac{d^2\mathbf{q}}{(2\pi)^2} T \ln \left( 1 - e^{-\varepsilon_{\mathbf{q}}/T} \right) = -\frac{\zeta(3)T^3}{2\pi(v^d)^2}, \quad (69)$$

where the dispersion relation is  $\varepsilon_{\mathbf{q}} = v^d|\mathbf{q}|$  and  $\zeta(x)$  is the Riemann zeta function. At finite temperature, we take into account the fluctuation contribution to the number density. The total fermion density  $n$  can be modified to

$$n \equiv n_0 - \frac{\partial \Omega_2^d}{\partial \mu} = n_0 - \frac{\zeta(3)T^3}{\pi(v^d)^3} \frac{\partial v^d}{\partial \mu}, \quad (70)$$

which reduces to  $n_0$  at zero temperature.

## B. KT and VAL melting transitions

In the following, we're going to explore the transition features in the 1/2-spin system with  $d$ -wave paring. The KT and VAL melting temperatures are both directly related to the stiffness  $J = \rho^d/(4m)$  in the following way [33–35, 49]:

$$T_{\text{KT}} = \frac{\pi}{2} J^d(T_{\text{KT}}), \quad T_{\text{M}} = 0.3 J^d(T_{\text{M}}). \quad (71)$$

Then, if the gap equation Eq.(49), number density equation Eq.(70) and critical temperature equations Eq.(71) are solved self-consistently, we can calculate  $T_{\text{KT}}$  and  $T_{\text{M}}$ .

We will consider two distinct cases, one is the balanced Fermi gases and another is the imbalanced Fermi gases.

### 1. Balanced Fermi gases

For the balanced fermion gases with  $\delta\mu = 0$ , the numerical results are shown in Fig.3. The transition temperatures  $T_{\text{KT}}$  and  $T_{\text{M}}$  are nearly constants in the deep BEC region,  $T_{\text{KT}} = 0.125\epsilon_F$  and  $T_{\text{M}} = (0.6/\pi)T_{\text{KT}}$ ; just as what we found in the  $p$ -wave pairing case. The chemical potentials at  $T_{\text{M}}$  and  $T_{\text{KT}}$  are almost the same; similarly, the order parameters at  $T_{\text{M}}$  and  $T_{\text{KT}}$  are also almost the same.

In the  $d$ -wave paring case, the non-analyticity is also found at the BCS-BEC transition point which is defined at  $\mu = 0$ . To see this, we can take the similar argument as we gave for the  $p$ -wave pairing case. We explore the property of the most relevant quantity  $\zeta_0^d$  around  $\mu = 0$ . The derivative of  $\zeta_0^d$  with respect to  $\mu$  is given by:

$$\frac{\partial \zeta_0^d}{\partial \mu} = \sum_{\mathbf{k}} \frac{\xi_{\mathbf{k}} |\Gamma^d(\mathbf{k})|^2}{4E_{\mathbf{k}}^4} \left[ \frac{3 \tanh\left(\frac{E_{\mathbf{k}}}{2T}\right)}{E_{\mathbf{k}}} - \frac{\text{sech}^2\left(\frac{E_{\mathbf{k}}}{2T}\right)}{2T} \right], \quad (72)$$

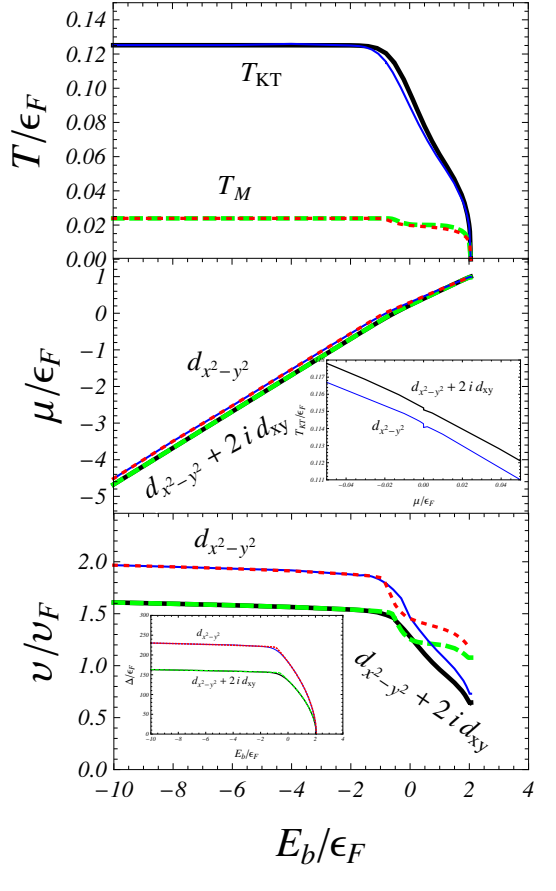


FIG. 3: (Color online) Upper panel: the transition temperatures,  $T_{\text{KT}}$  (solid lines) and  $T_{\text{M}}$  (dashed lines) as functions of the two-body binding energy  $E_b$  for both the isotropic  $d_{x^2-y^2} + 2id_{xy}$  pairing (black and green thick lines) and the anisotropic  $d_{x^2-y^2}$  pairing (blue and red thin lines). Lower panels: the chemical potential  $\mu$  and sound velocity  $v$  as functions of  $E_b$  at  $T_{\text{KT}}$  and  $T_{\text{M}}$ . The inserts are the zoom-in plot of  $T_{\text{KT}}$  with respect to  $\mu$  around the BCS-BEC transition point  $\mu = 0$  (the anisotropic result is shifted down by 0.001 for clearness) and the evolution of the order parameter  $\Delta$ , respectively. The parameters are the same as those used in Fig. 1.

which at  $\mu = 0$  is divergent logarithmically. This further induces non-analyticities in  $n$ ,  $T_{\text{KT}}$ ,  $T_{\text{M}}$ , etc. In the numerical results as shown in Fig. 3, the non-analyticities are not obvious for the chosen parameters  $k_0$  and  $k_1$ ; however, we can easily identify the non-analyticity in the inserted figure for  $T_{\text{KT}}$ .

Unlike the  $p$ -wave pairing case, the sound velocity for  $d$ -wave pairing does not show non-monotonicity: it is always a decreasing function when  $E_b$  goes from positive to negative values. This can be understood to Fig.4: As  $\zeta^d$  always increases faster than  $\rho^d$  with  $\mu$ , the sound velocity  $v^d$  decreases monotonously with the binding energy  $E_b$ .

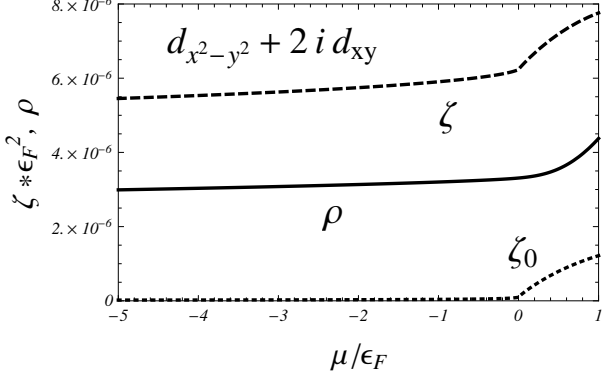


FIG. 4: An illumination of the functions  $\zeta_0^d$ ,  $\zeta^d$  and  $\rho^d$  involved in the sound velocity  $v$  with the chemical potential  $\mu$  at fixed temperature  $T = 0.12\epsilon_F$  and order parameter  $\Delta = 150\epsilon_F$  which are approximately the values at the BEC-side Kosterlitz-Thouless transition with isotropic  $d_{x^2-y^2} + 2id_{xy}$  pairing. The parameters are the same as in Fig. 1.

## 2. Mismatched Fermi gases

In order to study the effect of mismatched Fermi surface characterized by  $\delta\mu$  on KT and VAL melting transitions, we choose a fixed binding energy  $E_b = -2\epsilon_F$  as an example which lies in the BEC region.

We plot the transition temperatures  $T_{KT}$  and  $T_M$ , the chemical potentials at  $T_{KT}$  and  $T_M$ , the order parameters  $\Delta$  at  $T_{KT}$  and  $T_M$  and the sound velocity  $v$  at  $T_{KT}$  and  $T_M$  as functions of  $\delta\mu$  in Fig. 5. As expected, all these quantities are decreasing when  $\delta\mu$  increases. For small  $\delta\mu$ , the decreasing effect is not obvious; but for large  $\delta\mu$ , they almost linearly decrease with  $\delta\mu$  and finally reach a critical point  $\delta\mu_c \sim 3\epsilon_F$  beyond which no pairing state exists and the KT and VAL melting temperatures both meet zero at this point.

## IV. SUMMARY

In this work, the features of the topological Kosterlitz-Thouless and vortex-antivortex lattice melting transitions are explored in detail for fermionic systems with higher partial wave pairings, that is,  $p$ -wave pairings and  $d$ -wave pairings. At finite temperature, the contribution from Gaussian fluctuation (mainly  $\theta$  mode) is counted in the thermodynamic potential by using pole approximation. The stiffness, which is involved in the calculation of the Gaussian contribution and is directly related to the transition temperatures  $T_{KT}$  and  $T_M$ , is obtained. The expression is verified numerically for and found to be exactly consistent with the universal result due to the Galilean invariance [31].

The main results from numerical calculations can be summarized as follows:

**(a)** For  $p$ -wave pairings, constant transition temperatures  $T_{KT}$  and  $T_M$  are found in the deep BEC region:  $T_{KT} = 0.0625\epsilon_F$  and  $T_M = (0.6/\pi)T_{KT}$ . The transition temperatures and the sound velocities are found to be continuous but non-analytic

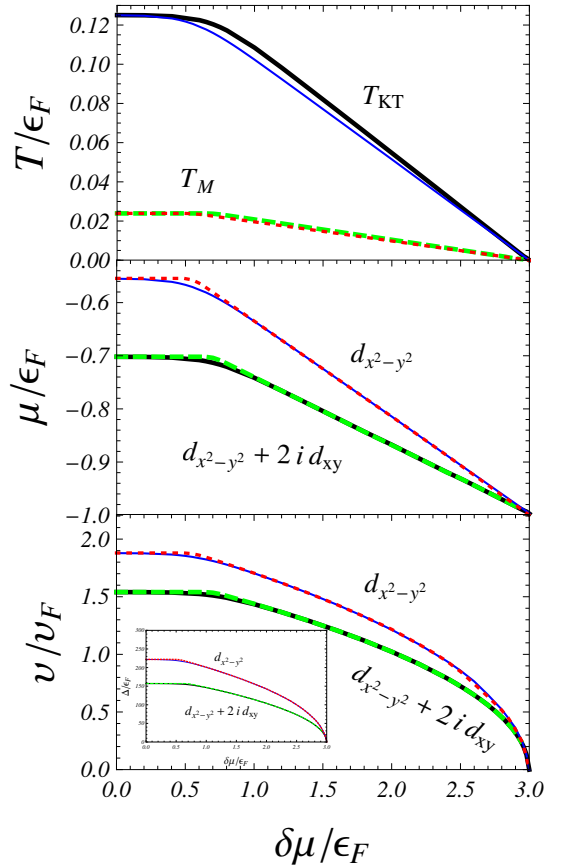


FIG. 5: (Color online) Upper panel: the transition temperatures,  $T_{KT}$  (solid lines) and  $T_M$  (dashed lines) as functions of the Zeeman field  $\delta\mu$  with a chosen binding energy  $E_b = -2\epsilon_F$  for both the isotropic  $d_{x^2-y^2} + 2id_{xy}$  pairing (black and green thick lines) and the anisotropic  $d_{x^2-y^2}$  pairing (blue and red thin lines). Lower panels: the chemical potential  $\mu$  and sound velocity  $v$  as functions of  $\delta\mu$  at  $T_{KT}$  and  $T_M$ . The insert is the evolution of the order parameter  $\Delta$ . The parameters are the same as in Fig. 1.

across the point  $\mu = 0$  where two topological transitions meet each other. For the anisotropic  $p_x$  pairing, the sound velocity is found to be also anisotropic in BCS region but nearly symmetric in the deep BEC region.

**(b)** For  $d$ -wave pairings, similar with the  $p$ -wave pairing case, constant transition temperatures  $T_{KT}$  and  $T_M$  are found in the deep BEC region. The transition temperatures and sound velocities are also found to be noncontinuous across the point  $\mu = 0$  which is consistent with our previous result that  $d$ -wave pairings usually gives higher divergent degrees than  $p$ -wave pairings [25]. Due to the exchange symmetry between  $k_x$  and  $k_y$ , the sound velocity is found to be isotropic even for the anisotropic  $d_{x^2-y^2}$  pairing. The mismatched Fermi surface can be introduced to the  $d$ -wave pairing systems and a critical mismatch is found where the transition temperatures becomes

zero.

### Acknowledgments

We thank Hui Hu for discussion. This work is supported by the Young 1000 Talents Program of China. G.C. and X.G.H.

are also supported by NSFC with Grant NO. 11535012 and NO. 11675041, and Scientific Research Foundation of State Education Ministry for Returned Scholars. G.C. is also supported by China Postdoctoral Science Foundation with Grant NO. KLH1512072.

### Appendix A: The expansion coefficients around small momenta for $\theta$ mode

In order to find the analytic form of the stiffness, we expand  $M_{11} + M_{22} - M_{12} - M_{21}$  for small  $\mathbf{q}$  at  $i\nu_n = 0$ . We take the  $d$ -wave pairing case as an example;  $p$ -wave pairing case is similar. The relevant term is

$$F(\mathbf{q}) = \sum_{\mathbf{k}, m} \frac{1}{[(i\tilde{\omega}_m)^2 - E_{\mathbf{k}-\mathbf{q}/2}^2][(i\tilde{\omega}_m)^2 - E_{\mathbf{k}+\mathbf{q}/2}^2]} \left\{ 2(i\tilde{\omega}_m - \xi_{\mathbf{k}-\mathbf{q}/2})(i\tilde{\omega}_m + \xi_{\mathbf{k}+\mathbf{q}/2})|\Gamma^d(\mathbf{k})|^2 - \Delta_{\mathbf{k}-\mathbf{q}/2}\Delta_{\mathbf{k}+\mathbf{q}/2}(\Gamma^{d*}(\mathbf{k}))^2 \right. \\ \left. - \Delta_{\mathbf{k}-\mathbf{q}/2}^* \Delta_{\mathbf{k}+\mathbf{q}/2}^*(\Gamma^d(\mathbf{k}))^2 \right\}, \quad (\text{A1})$$

where  $i\tilde{\omega}_m = i\omega_m - \delta\mu$ . Then, the first derivative of  $F(\mathbf{q})$  with respect to  $q_i$  ( $i = x, y$ ) is

$$\partial_{q_i} F(\mathbf{q}) = \sum_{\mathbf{k}, m} \frac{1}{[(i\tilde{\omega}_m)^2 - E_{\mathbf{k}-\mathbf{q}/2}^2][(i\tilde{\omega}_m)^2 - E_{\mathbf{k}+\mathbf{q}/2}^2]} \left\{ [\partial_{k_i} \xi_{\mathbf{k}-\mathbf{q}/2}(i\tilde{\omega}_m + \xi_{\mathbf{k}+\mathbf{q}/2}) + \partial_{k_i} \xi_{\mathbf{k}+\mathbf{q}/2}(i\tilde{\omega}_m - \xi_{\mathbf{k}-\mathbf{q}/2})]|\Gamma^d(\mathbf{k})|^2 \right. \\ \left. - \frac{1}{2}(-\Delta'_{\mathbf{k}-\mathbf{q}/2}\Delta_{\mathbf{k}+\mathbf{q}/2} + \Delta_{\mathbf{k}-\mathbf{q}/2}\Delta'_{\mathbf{k}+\mathbf{q}/2})(\Gamma^{d*}(\mathbf{k}))^2 - \frac{1}{2}(-\Delta'^*_{\mathbf{k}-\mathbf{q}/2}\Delta^*_{\mathbf{k}+\mathbf{q}/2} + \Delta^*_{\mathbf{k}-\mathbf{q}/2}\Delta'^*_{\mathbf{k}+\mathbf{q}/2})(\Gamma^d(\mathbf{k}))^2 \right\} \\ - \frac{1}{2[(i\tilde{\omega}_m)^2 - E_{\mathbf{k}-\mathbf{q}/2}^2]^2[(i\tilde{\omega}_m)^2 - E_{\mathbf{k}+\mathbf{q}/2}^2]^2} \left\{ (E_{\mathbf{k}-\mathbf{q}/2}^2)'[(i\tilde{\omega}_m)^2 - E_{\mathbf{k}+\mathbf{q}/2}^2] - (E_{\mathbf{k}+\mathbf{q}/2}^2)'[(i\tilde{\omega}_m)^2 - E_{\mathbf{k}-\mathbf{q}/2}^2] \right\} \\ \left\{ 2(i\tilde{\omega}_m - \xi_{\mathbf{k}-\mathbf{q}/2})(i\tilde{\omega}_m + \xi_{\mathbf{k}+\mathbf{q}/2})|\Gamma^d(\mathbf{k})|^2 - \Delta_{\mathbf{k}-\mathbf{q}/2}\Delta_{\mathbf{k}+\mathbf{q}/2}(\Gamma^{d*}(\mathbf{k}))^2 - \Delta_{\mathbf{k}-\mathbf{q}/2}^*\Delta_{\mathbf{k}+\mathbf{q}/2}^*(\Gamma^d(\mathbf{k}))^2 \right\}. \quad (\text{A2})$$

Keeping in mind the evenness of the function  $[(i\tilde{\omega}_m)^2 - E_{\mathbf{k}-\mathbf{q}/2}^2][(i\tilde{\omega}_m)^2 - E_{\mathbf{k}+\mathbf{q}/2}^2]$  for  $\mathbf{q}$ , we can evaluate the second derivatives of  $F(\mathbf{q})$  around  $\mathbf{q} = 0$  as

$$\partial_{q_i}^2 F(\mathbf{q})|_{\mathbf{q}=0} = \sum_{\mathbf{k}, m} \frac{1}{[(i\tilde{\omega}_m)^2 - E_{\mathbf{k}}^2]^2} \left\{ [\xi_{\mathbf{k}} \partial_{k_i}^2 \xi_{\mathbf{k}} + 3(\partial_{k_i} \xi_{\mathbf{k}})^2]|\Gamma^d(\mathbf{k})|^2 + \frac{\Delta^2}{4}(|\Gamma^d(\mathbf{k})|^4)'' \right\} + \frac{4|\Gamma^d(\mathbf{k})|^2}{[(i\tilde{\omega}_m)^2 - E_{\mathbf{k}}^2]^3} \left[ \xi_{\mathbf{k}} \partial_{k_i} \xi_{\mathbf{k}} + \frac{1}{2}(|\Delta_{\mathbf{k}}|^2)' \right]^2 \quad (\text{A3})$$

Finally, the summation of the Matsubara frequency can be completed to give the following result:

$$\partial_{q_i}^2 F(\mathbf{q})|_{\mathbf{q}=0} = \sum_{\mathbf{k}, s=\pm} \left\{ [\xi_{\mathbf{k}} \partial_{k_i}^2 \xi_{\mathbf{k}} + 3(\partial_{k_i} \xi_{\mathbf{k}})^2]|\Gamma^d(\mathbf{k})|^2 + \frac{\Delta^2}{4}(|\Gamma^d(\mathbf{k})|^4)'' \right\} \left( \frac{\tanh(\frac{E_{\mathbf{k}}+s\delta\mu}{2T})}{8E_{\mathbf{k}}^3} - \frac{\text{sech}^2(\frac{E_{\mathbf{k}}+s\delta\mu}{2T})}{16TE_{\mathbf{k}}^2} \right) \\ + \left[ \xi_{\mathbf{k}} \partial_{k_i} \xi_{\mathbf{k}} + \frac{1}{2}(|\Delta_{\mathbf{k}}|^2)' \right]^2 |\Gamma^d(\mathbf{k})|^2 \left( -\frac{3 \tanh(\frac{E_{\mathbf{k}}+s\delta\mu}{2T})}{8E_{\mathbf{k}}^5} + \frac{3 \text{sech}^2(\frac{E_{\mathbf{k}}+s\delta\mu}{2T})}{16TE_{\mathbf{k}}^4} + \frac{\tanh(\frac{E_{\mathbf{k}}+s\delta\mu}{2T}) \text{sech}^2(\frac{E_{\mathbf{k}}+s\delta\mu}{2T})}{16T^2E_{\mathbf{k}}^3} \right). \quad (\text{A4})$$

For  $s$ -wave or  $p$ -wave pairings, we only need to change the corresponding gamma functions  $\Gamma^d(\mathbf{k})$  to  $\Gamma^{s/p}(\mathbf{k})$  and set  $\delta\mu \equiv 0$  for  $p$ -wave systems. For  $s$ -wave pairing, the expressions are simplified as  $\Gamma^s(\mathbf{k}) = 1$ . Then Eq.(A3) for  $s$ -wave pairing can be simplified to the following expression:

$$\partial_{q_i}^2 F(\mathbf{q})|_{\mathbf{q}=0} = \sum_{\mathbf{k}, m} \frac{\xi_{\mathbf{k}} \partial_{k_i}^2 \xi_{\mathbf{k}} + 3(\partial_{k_i} \xi_{\mathbf{k}})^2}{[(i\tilde{\omega}_m)^2 - E_{\mathbf{k}}^2]^2} + \frac{4(\xi_{\mathbf{k}} \partial_{k_i} \xi_{\mathbf{k}})^2}{[(i\tilde{\omega}_m)^2 - E_{\mathbf{k}}^2]^3}. \quad (\text{A5})$$

Using the following identities,

$$-\frac{\partial}{\partial\mu}\frac{\xi_{\mathbf{k}}}{[(i\tilde{\omega}_m)^2 - E_{\mathbf{k}}^2]^2} = \frac{1}{[(i\tilde{\omega}_m)^2 - E_{\mathbf{k}}^2]^2} + \frac{4\xi_{\mathbf{k}}^2}{[(i\tilde{\omega}_m)^2 - E_{\mathbf{k}}^2]^3}, \quad (\text{A6})$$

$$\begin{aligned} -\sum_{\mathbf{k},m}(\partial_{k_i}\xi_{\mathbf{k}})^2\frac{\partial}{\partial\mu}\frac{\xi_{\mathbf{k}}}{[(i\tilde{\omega}_m)^2 - E_{\mathbf{k}}^2]^2} &= \sum_{\mathbf{k},m}(\partial_{k_i}\xi_{\mathbf{k}})^2\frac{\partial}{\partial\xi_{\mathbf{k}}}\frac{\xi_{\mathbf{k}}}{[(i\tilde{\omega}_m)^2 - E_{\mathbf{k}}^2]^2} = \frac{2m}{4\pi}\sum_m\int_0^\infty d\xi_{\mathbf{k}}(\partial_{k_i}\xi_{\mathbf{k}})^2\frac{\partial}{\partial\xi_{\mathbf{k}}}\frac{\xi_{\mathbf{k}}}{[(i\tilde{\omega}_m)^2 - E_{\mathbf{k}}^2]^2} \\ &= -\frac{2m}{4\pi}\sum_m\int_0^\infty d\xi_{\mathbf{k}}\partial_{k_i}^2\xi_{\mathbf{k}}\frac{\xi_{\mathbf{k}}}{[(i\tilde{\omega}_m)^2 - E_{\mathbf{k}}^2]^2} = -\sum_{\mathbf{k},m}\partial_{k_i}^2\xi_{\mathbf{k}}\frac{\xi_{\mathbf{k}}}{[(i\tilde{\omega}_m)^2 - E_{\mathbf{k}}^2]^2}, \end{aligned} \quad (\text{A7})$$

the final result can be shown to be

$$\partial_{q_i}^2 F(\mathbf{q})|_{\mathbf{q}=0} = \sum_{\mathbf{k},m} \frac{2(\partial_{k_i}\xi_{\mathbf{k}})^2}{[(i\tilde{\omega}_m)^2 - E_{\mathbf{k}}^2]^2} = \sum_{\mathbf{k}} \frac{\mathbf{k}^2}{4m^2 E_{\mathbf{k}}^2} \left( \frac{\tanh(\frac{E_{\mathbf{k}}}{2T})}{E_{\mathbf{k}}} - \frac{\operatorname{sech}^2(\frac{E_{\mathbf{k}}}{2T})}{2T} \right), \quad (\text{A8})$$

at  $\delta\mu = 0$ . This is equivalent to the explicit form given in Ref. [49].

---

[1] D. M. Eagles, Phys. Rev. **186**, 456 (1969).

[2] A. J. Leggett, *In Modern Trends in the Theory of Condensed Matter*, Springer-Verlag, Berlin, 1980.

[3] P. Nozieres and S. Schmitt-Rink, J. Low Temp. Phys. **59**, 195 (1985).

[4] C. A. R. Sa de Melo, M. Randeria, and J. R. Engelbrecht, Phys. Rev. Lett. **71**, 3202 (1993).

[5] J. R. Engelbrecht, M. Randeria, and C. A. R. Sa de Melo, Phys. Rev. **B55**, 15153 (1997).

[6] M. Randeria, J.-M. Duan, and L.-Y. Shieh, Phys. Rev. Lett. **62**, 981 (1989).

[7] M. Randeria, J.-M. Duan, and L.-Y. Shieh, Phys. Rev. **B41**, 327 (1990).

[8] V. M. Loktev, R. M. Quick, and S. G. Sharapov, Phys. Rept. **349**, 1 (2001).

[9] Q. Chen, J. Stajic, S. Tan, and K. Levin, Phys. Rept. **412**, 1 (2005).

[10] S. Giorgini, L. P. Pitaevskii, and S. Stringari, Rev. Mod. Phys. **80**, 1215 (2008).

[11] V. Gurarie and L. Radzihovsky, Ann. Phys. (N.Y.) **322**, 2 (2007).

[12] R. Combescot, M. Yu. Kagan, and S. Stringari, Phys. Rev. **A74**, 042717 (2006).

[13] L. Belkhir and M. Randeria, Phys. Rev. **B45**, 5087 (1992).

[14] L. Belkhir and M. Randeria, Phys. Rev. **B49**, 6829 (1994).

[15] M. Greiner, C. A. Regal, and D. S. Jin, Nature (London) **426**, 537 (2003).

[16] S. Jochim, M. Bartenstein, A. Altmeyer, G. Hendl, S. Riedl, C. Chin, J. Hecker Denschlag, and R. Grimm, Science **302**, 2101 (2003).

[17] M. W. Zwierlein, J. R. Abo-Shaeer, A. Schirotzek, C. H. Schunck, and W. Ketterle, Nature (London) **435**, 1047 (2003).

[18] N. Read and D. Green, Phys. Rev. **B61**, 10267 (2000).

[19] S. S. Botelho and C. A. R. Sá de Melo, J. Low Temp. Phys. **140**, 409 (2005).

[20] S. S. Botelho and C. A. R. Sá de Melo, Phys. Rev. **B71**, 134507 (2005).

[21] V. Gurarie, L. Radzihovsky, and A. V. Andreev, Phys. Rev. Lett. **94**, 230403 (2005).

[22] C.-H. Cheng and S.-K. Yip, Phys. Rev. Lett. **95**, 070404 (2005).

[23] M. Iskin and C. A. R. Sa de Melo, Phys. Rev. Lett. **96**, 040402 (2006).

[24] M. Iskin and C. A. R. Sa de Melo, Phys. Rev. **A74**, 013608 (2006).

[25] G. Cao, L. He, and P. Zhuang, Phys. Rev. **A87**, 013613 (2013).

[26] V. Makhalov, K. Martiyanov, and A. Turlapov, Phys. Rev. Lett. **112**, 045301 (2014).

[27] B. Fröhlich, M. Feld, E. Vogt, M. Koschorreck, W. Zwerger, and M. Köhl, Phys. Rev. Lett. **106**, 105301 (2011).

[28] W. Ong, C.-Y. Cheng, I. Arakelyan, and J. E. Thomas, Phys. Rev. Lett. **114**, 110403 (2015).

[29] M. G. Ries, A. N. Wenz, G. Zurn, L. Bayha, I. Boettcher, D. Kedar, P. A. Murthy, M. Neidig, T. Lompe, and S. Jochim, Phys. Rev. Lett. **114**, 230401 (2015).

[30] A. T. Sommer, L. W. Cheuk, M. J. H. Ku, W. S. Bakr, and M. W. Zwierlein, Phys. Rev. Lett. **108**, 045302 (2012).

[31] A. J. Leggett, *Quantum liquid*, Oxford University press, Oxford (2006).

[32] S. Doniach and B. A. Huberman, Phys. Rev. Lett. **42**, 1169 (1979).

[33] V. L. Berezinskii, Sov. Phys. JETP **32**, 493 (1971); **34**, 610 (1972); J. M. Kosterlitz and D. Thouless, J. Phys. C **5**, L124 (1972); **6**, 1181 (1973).

[34] D. R. Nelson and B. I. Halperin, Phys. Rev. **B19**, 2457 (1979).

[35] A. P. Young, Phys. Rev. **B19**, 1855 (1979).

[36] V. M. Loktev, R. M. Quick, and S. G. Sharapov, Phys. Rep. **349**, 1 (2001).

[37] D. S. Petrov, M. A. Baranov, and G. V. Shlyapnikov, Phys. Rev. **A67**, 031601(R) (2003).

[38] W. Zhang, G.-D. Lin, and L.-M. Duan, Phys. Rev. **A78**, 043617 (2008).

[39] M. Iskin and C. A. R. Sa de Melo, Phys. Rev. Lett. **103**, 165301 (2009).

[40] J. Tempere, S. N. Klimin, and J. T. Devreese, Phys. Rev. **A79**, 053637 (2009).

[41] S. N. Klimin, J. Tempere, and J. T. Devreese, New J. Phys. **14**,

103044 (2012).

[42] L. Salasnich, P. A. Marchetti, and F. Toigo, Phys. Rev. **A88**, 053612 (2013).

[43] P. A. Murthy, I. Boettcher, L. Bayha, M. Holzmann, D. Kedar, M. Neidig, M. G. Ries, A. N. Wenz, G. Zurn, and S. Jochim, Phys. Rev. Lett. **115**, 010401 (2015).

[44] L. He and X.-G. Huang, Phys. Rev. Lett. **108**, 145302 (2012).

[45] J. P. A. Devreese, J. Tempere, and C. A.R. Sa de Melo, Phys. Rev. Lett. **113**, 165304 (2014).

[46] J. P. A. Devreese, J. Tempere, and C. A.R. Sa de Melo, Phys. Rev. A **92**, 043618 (2015).

[47] Y. Xu and C. Zhang, Phys. Rev. Lett. **114**, 110401 (2015).

[48] Y. Cao, X.-J. Liu, L. He, G.-L. Long, and H. Hu, Phys. Rev. **A91**, 023609 (2015).

[49] S. S. Botelho and C. A. R. Sá de Melo, Phys. Rev. Lett. **96**, 040404 (2006).

[50] H. Hu, X.-J. Liu, and P. D. Drummond, Euro- phys. Lett. **74**, 574 (2006).

[51] R. B. Diener, R. Sensarma, and M. Randeria, Phys. Rev. **A77**, 023626 (2008).

[52] L. He, H. Lu, G. Cao, H. Hu, and X.J. Liu, Phys. Rev. **A92**, 023620 (2015).

[53] G. Bighin and L. Salasnich, Phys. Rev. **B93**, 014519 (2016).

[54] B. C. Mulkerin, L. He, P. Dyke, C. J. Vale, X.-J. Liu, and H. Hu, arXiv:1702.07091.

[55] J. P. A. Devreese, J. Tempere, and C. A. R. Sá de Melo, Phys. Rev. Lett. **113**, 165304 (2014).

[56] G. Sarma, J. Phys. Chem. Solid **24**, 1029 (1963).

[57] A. I. Larkin and Yu. N. Ovchinnikov, Sov. Phys. JETP **20**, 762 (1965).

[58] P. Fulde and R. A. Ferrell, Phys. Rev **135**, A550 (1964).

[59] S. Takada and T. Izuyama, Prog. Theor. Phys. **41**, 635 (1969).

[60] H. Zhai, Rept. Prog. Phys. **78**, 026001 (2015).